

Article

# Local Retrofit of Reinforced Concrete Structures by the ACM System

Stefano Sorace <sup>1</sup> , Gloria Terenzi <sup>2,\*</sup> and Elena Fuso <sup>1</sup>

<sup>1</sup> Polytechnic Department of Engineering and Architecture, University of Udine, 33100 Udine, Italy; stefano.sorace@uniud.it (S.S.); elena.fuso@uniud.it (E.F.)

<sup>2</sup> Department of Civil and Environmental Engineering, University of Florence, 50123 Firenze, Italy

\* Correspondence: gloria.terenzi@unifi.it; Tel.: +39-55-275-8887

**Abstract:** During the last decades, low architectural impact strategies have been increasingly adopted in the seismic retrofit of reinforced concrete structures. Among the emerging technologies in this field, the active lateral confinement of columns, beams, and beam-to-column joints is gaining growing attention thanks to the localization of the interventions only on the members in unsafe conditions, the resulting small increase in size, and the limited demolition required for installation. The study presented herein is focused on the application of a highly performing confinement technology, named as ACM (Active Confinement of Masonry), which was conceived more than twenty years ago in Italy for masonry structures, and then successfully applied to reinforced concrete ones. A representative case study is examined in detail herein, i.e., a school built in the early 1960s in the Friuli Venezia Giulia area in Italy. A seismic assessment analysis of the building is carried out in its current state, also supported by preliminary diagnostic investigations, which highlights several seismic deficiencies, especially in terms of shear response of columns and beams. Thus, a retrofit hypothesis based on the installation of the ACM system is proposed, which allows attaining a substantial improvement in the seismic response capacities, while maintaining limited architectural intrusion. A detailed description of the case study characteristics and a synthesis of the time-history seismic analyses developed in original conditions are presented in this article, along with the design criteria, drawings of the interventions, and an evaluation of the resulting performance enhancement in retrofitted configuration.

**Keywords:** active confinement; reinforced concrete structures; local seismic retrofit strategies; ACM method; time-history analysis



**Citation:** Sorace, S.; Terenzi, G.; Fuso, E. Local Retrofit of Reinforced Concrete Structures by the ACM System. *Buildings* **2021**, *11*, 575. <https://doi.org/10.3390/buildings11120575>

Academic Editor: David Arditi

Received: 30 October 2021

Accepted: 22 November 2021

Published: 24 November 2021

**Publisher's Note:** MDPI stays neutral with regard to jurisdictional claims in published maps and institutional affiliations.



**Copyright:** © 2021 by the authors. Licensee MDPI, Basel, Switzerland. This article is an open access article distributed under the terms and conditions of the Creative Commons Attribution (CC BY) license (<https://creativecommons.org/licenses/by/4.0/>).

## 1. Introduction

Frame buildings with a reinforced concrete (RC) structure designed in the 1960s normally show poor response capacities to earthquakes due to the absence of specific anti-seismic measures in their original design conception and detailing [1–3].

Innovative seismic retrofit strategies are now increasingly adopted for this class of building to limit architectural impact, working times, and costs of the interventions, as well as to upgrade their structural and non-structural seismic performance, as compared to traditional rehabilitation techniques. Among these innovative strategies, the ones based on the notion of active lateral confinement (ALC) of RC members are gaining growing attention from the academic and professional communities. Starting from early studies on concrete failure under biaxial compressive stress states [1], the concept of lateral confinement as a tool for increasing strength and ductility of RC members has been theoretically fixed by fundamental research contributions [4–8] and has progressively evolved up to date. This prompted the conception of several passive lateral confinement (PLC) retrofit strategies, based on the external installation of transversal steel reinforcements like hoops, straps, cages [9–15] or jackets [16–22], RC jackets [23–26], mortar jackets [27], or, after the successful

introduction of fibre reinforced polymer (FRP) materials in the broad field of structural rehabilitation, of perimeter wrapping with FRP layers or fabric sheets [28–34]. As an alternative, ALC technologies, which differ from PLC ones for the application of an initial confining pressure obtained by prestressing the lateral surface of the considered members—inspired to the classical “active hooping” strategy applied for centuries to stone and masonry columns—have been recently extended to RC structures too [35–48].

Among the ALC technologies, a pioneer role has been played by the ACM (Active Confinement of Masonry, “CAM” in Italian, registered trademark) technology, ideated more than twenty years ago in Italy for masonry structures [49,50], and later successfully adapted with effective results to RC ones. The system consists of stainless steel ribbons, shaped like thin strips, embracing and tying walls (masonry structures) or beams, columns, and beam-to-column joints (RC frame structures) by means of closed loops passing through transverse holes. The active confinement effect is generated by pre-tensioning the strips. The additional local stress states induced by pre-tension in the contact zones with the structural members are distributed by means of connection elements, such as flat and funnel-type plates, and angles.

Like other ALC technologies applied to RC structures, the advantages offered by the ACM system are represented by the localisation of demolitions in the perimeter zones around the beams, columns, and joints to be retrofitted, and a practically null addition of masses in the total dead mass computation for the building (Figure 1). Consistently, architectural intrusion, working times, and costs are remarkably reduced compared to traditional rehabilitation solutions, and benefits are obtained also in terms of seismic structural weights. At the same time, a distinguishing characteristic of the ACM system, in comparison to other ALC strategies, is that the strips are made of high-strength stainless steel, which helps limiting their thickness below one millimetre per strip while guaranteeing high pre-stress levels and preserving them from oxidation during their in-place lifespan. Moreover, the strips can be installed on beams, columns, and joints without discontinuities, and the system offers, in addition to lateral confinement, significant supplemental steel reinforcement.

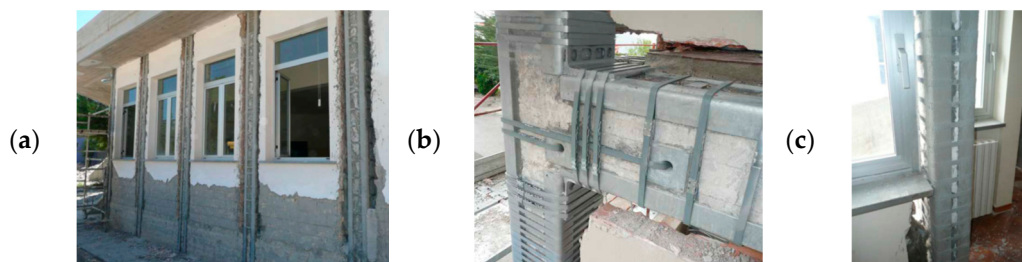


**Figure 1.** Images of a typical ACM-based retrofit intervention on a building with RC frame structure: view of a façade (a), a beam-to-column joint (b), and a column situated in proximity to two windows (c)—pictures taken from [50].

The study presented herein concerns a hypothesis of application of the ACM system to an Italian building of the early 1960s with RC frame structure, characterised by the typical seismic vulnerabilities of a wide class of reinforced concrete structures belonging to that period. As illustrated in Section 2, this was assessed by a non-linear time-history analysis carried out in current conditions, the results of which highlight remarkably unsafe stress states in most members at the basic design earthquake (BDE) level of seismic action, especially in terms of shear. Low ductility capacities of columns and beams also emerge in flexure, and unsafe conditions for about 40% of beam-to-column joints.

The ACM-based retrofit solution conceived for the case study building allows attaining safe stress states and a notably increased ductility in the retrofitted members, with limited demolition works of infills and partitions in contact with them and relatively low structural intervention costs, as discussed in Section 3.

## 2. Case Study Building

The considered building is a school situated in the town of Tolmezzo, Friuli-Venezia Giulia region, Italy. Its structural design dates back to 1960, and the construction works were completed in 1961. The general characteristics of the building and the results of the seismic assessment analysis carried out in current conditions are summarised below.

### 2.1. Geometrical and Structural Characteristics

The building has a rectangular plan, sized 13.5 m × 32.8 m, and is organised in four storeys above ground, with inter-storey heights of 3.36 m (ground storey), 3.65 (first), 3.62 (second), and 2.57 m (measured at the under-roof top). The structural plans of the first, second, and third floors and the roof are shown in Figures 2–5.

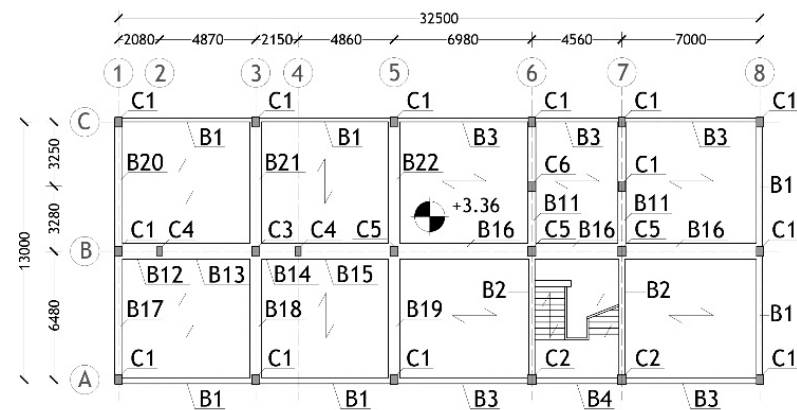


Figure 2. First floor structural plan.

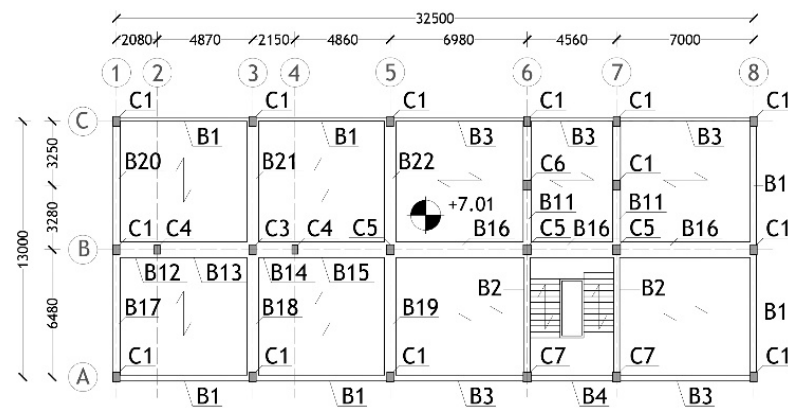


Figure 3. Second floor structural plan.

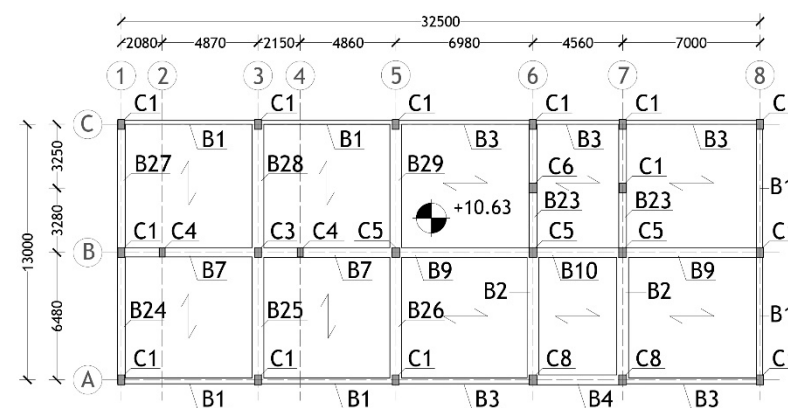


Figure 4. Third floor structural plan.

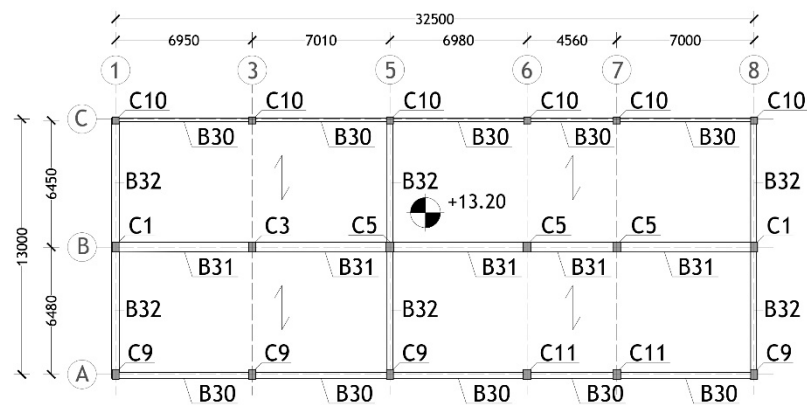


Figure 5. Roof structural plan.

The structure of the storey floors is made of 280 mm-high and 80 mm-wide RC joists parallel to the transversal direction in plan in the two left frame spans, and parallel to the longitudinal direction in the three remaining frame spans. The joists are placed at a mutual distance of 700 mm, as determined by the interposed clay lug bricks, and a 40 mm thick upper RC slab. The roof floor structure is made of “SAPAL”-type 370 mm-high reinforced clay lug bricks, integrated by on-site cast 350 mm-high RC ribs placed at a mutual distance of 1250 mm, and a 50 mm thick upper RC slab. Foundations are constituted by a mesh of inverse T-beams, with heights and flanges ranging from 700 mm to 1000 mm, and from 600 mm to 800 mm, respectively.

As part of the OSS (Seismic Observatory of Structures) programme promoted by the Italian Department of Civil Protection to structurally assess and monitor public buildings [51], a careful on-site mechanical investigation campaign was carried out on the case study one [52]. This campaign consisted of concrete cover demolitions (Figure 6a), pacometer tests (Figure 6b), and extraction of samples, for the reinforcing bars, and core drillings (Figure 7a) and Son-Reb tests (i.e., combined sclerometer—Figure 7b—and ultrasonic—Figure 7c—tests) for concrete.

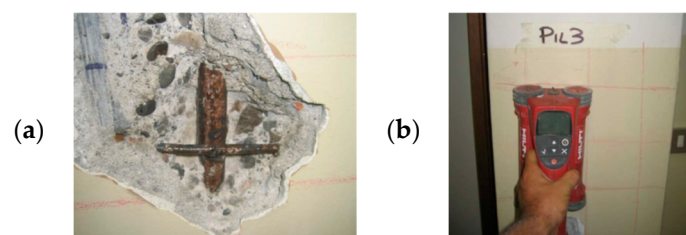


Figure 6. Images of a concrete cover demolition (a) and a pacometer test (b).

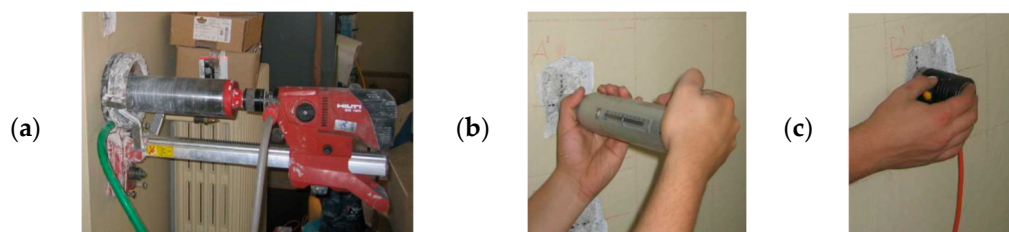


Figure 7. Images of a concrete core drilling (a), a sclerometer test (b), and an ultrasonic test (c).

The results of the tests highlighted the average values of yielding and ultimate stress values,  $f_{sy}$  and  $f_{su}$ , of 380 MPa and 500 MPa, respectively, and Young’s modulus,  $E_s$ , of 204,000 MPa for steel; and the average values of cylindrical compressive strength,  $f_c$ , equal

to 20.3 MPa, Young's modulus,  $E_c$ , of 21.500 MPa, and strains at peak stress and at collapse,  $\epsilon_c$ , and  $\epsilon_{cu}$ , equal to 0.00156 and 0.00402, respectively, for concrete.

## 2.2. Time-History Evaluation Analysis

The seismic response of the building was evaluated by means of the finite element model displayed in Figure 8, generated by the SAP2000NL calculus program [53]. Concrete-type frame elements were used to model beams and columns, and shell elements for the flights of stairs. The in-plan axial stiffness of the floors was simulated by means of equivalent horizontal braces. The model does not include infills in contact with the structural members because the assessment analysis was essentially focused on the building performance at the BDE, the peak lateral displacements relevant to which would significantly damage them, as discussed below, thus, practically annulling the contribution of infills to the seismic response.

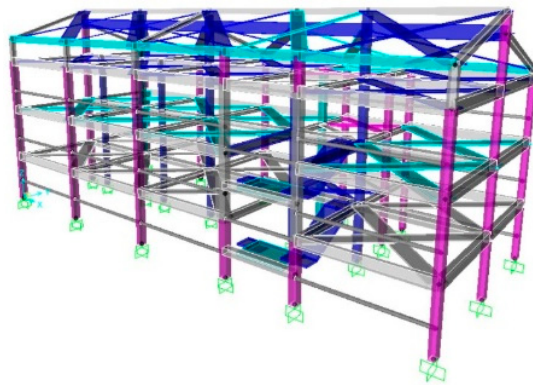


**Figure 8.** Finite element model of the structure.

The finite element model shown in Figure 8 was used for the analysis of the structure both in current state and in ACM-retrofitted conditions; the mechanical characteristics of concrete were changed when passing from the former to the latter, according to the criteria presented in Section 3.

A modal analysis of the structure was carried out in the first step of the assessment study, which highlighted three prevailing modes, and namely: a first translational mode along the longitudinal axis in plan, with vibration period of 0.32 s; and a second and a third mixed translational along the transversal axis in plan-rotational around the vertical axis modes, with periods of 0.23 s and 0.16 s, respectively. Nine modes are needed to obtain a summed effective modal mass greater than 85% of the total seismic mass of the building along the longitudinal (95%) and transversal (87%) axes, as well as around the vertical one (86%).

The non-linear time-history analyses were developed by adopting lumped plastic hinges at the end sections of beams, governed by a Takeda-type hysteretic relationship [54] and fibre-type plastic hinges—composed of concrete-type fibres and steel-type fibres—at the end sections of columns. For the latter, which allow an accurate consideration of the interaction between axial force and biaxial bending moment, a Mander-type [7] backbone curve and a Takeda-type hysteretic model were assumed for the concrete fibres, and a strain hardening elasto-plastic skeleton curve with hysteretic kinematic behaviour for the reinforcing steel fibres. A typical fibre model mesh of a column cross section is drawn in Figure 9, where the reinforcing bars are located by red dots encased in black circles.

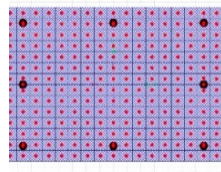


Figure 9. Fibre model of a column cross section.

The accelerograms used in the input for the time-history analyses were generated in seven groups of two horizontal components from the pseudo-acceleration response spectra referred to the municipality of Tolmezzo. In each analysis, a different pair of horizontal components was used in the input. The results were elaborated in mean terms over the response to the seven pairs. Attention is focused here on the response to the BDE, with a 10% probability of being exceeded over the reference time period  $V_R$ , fixed at 75 years by Italian Standards for school buildings [55]. The relevant response spectrum, referred to the soil conditions identified for the site of the building, and characterised by a peak ground acceleration of 0.284 g, is shown in Figure 10.

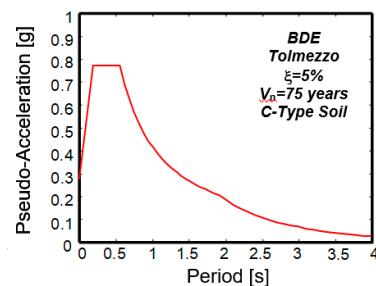
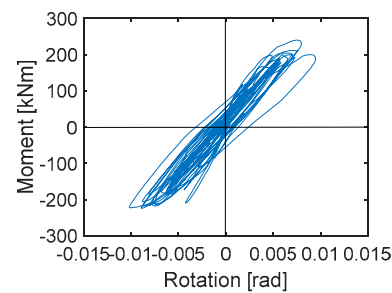


Figure 10. BDE-scaled pseudo-acceleration response spectrum for Tolmezzo.

A synthesis of the results of the analyses shows that the members in unsafe conditions are: 54 out of 84 columns in shear (namely, by referring to the plans in Figure 2 through Figure 5, 23 C1, 2 C2, 4 C3, 4 C4, 4 C5, 2 C6, 2 C7, 2 C8, 4 C9, 4 C10, and 2 C11-type columns), and 43 in combined axial force/biaxial flexure (21 C1, 2 C2, 4 C3, 2 C4, 10 C5, 2 C7, and 2 C8), with the maximum demand/capacity ratio ( $DCR$ ) values of 3.49 (shear) and 2.26 (combined axial force/biaxial flexure); 42 out of 73 beams in shear (14 B1, 4 B2, 15 B3, 3 B4, 4 B7, 1 B9, and 1 B10-type beams), and 32 (14 B1, 4 B2, 13 B3, and 1 B9) in flexure, with the maximum  $DCRs$  of 2.6 (shear) and 2.01 (flexure); and 25 out of 60 beam-to-column joints (by referring to the nomenclature reported in Section 3.1, 3 B, 3 D, 3 H, 3 N, 3 P, 2 C, 2 G, 2 I, 2 O, 1 E, and 1 F-type joints), with the maximum  $DCRs$  of 2.74. At the same time, safe conditions are evaluated for the foundation beams, both in flexure and shear.

For the example of the plastic demand in columns, the bending moment-rotation cyclic response around the strong flexural axis of C1 column situated in the A5 alignment on the ground storey is plotted in Figure 11 for the most demanding of the seven input accelerograms.

The energy response time-histories of the structure obtained for the same input ground motion are graphed in Figure 12, highlighting a similar contribution of the plastic energy related to the inelastic response of the RC members and the modal (i.e., viscous damping matrix-related) energy dissipated by the structure.



**Figure 11.** Bending moment-rotation response of C1 ground storey column belonging to A5 alignment around its strong flexural axis.

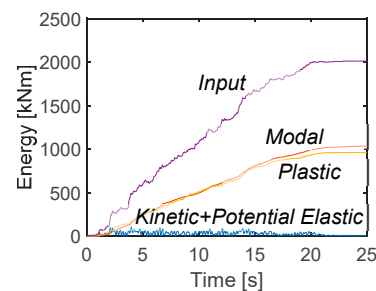


**Figure 12.** Energy time-histories of the structure.

The response in terms of lateral displacements is assessed by the maximum inter-storey drift values equal to about 1.3% of the inter-storey height in the longitudinal direction in plan, and 1.05% in the transversal direction, at the BDE. The corresponding values at the Serviceability Design Earthquake (SDE), characterised by 63% probability of being exceeded over  $V_R$ , are equal to 0.55% and 0.46%, respectively. Based on these results, negligible damage to non-structural elements (infills, partitions, finishes, and plants) is assessed at the SDE, and repairable damage at the BDE. This highlights an acceptable lateral displacement performance of the building, which does not prompt any interventions aimed at significantly increasing the horizontal translational stiffness of the structure.

In view of this, as well as of the remaining data drawn from the seismic assessment analysis in current conditions, a retrofit strategy aimed at improving the response capacities of beams, columns, and beam-to-column joints by means of local strengthening interventions, like the ACM-based one, was identified as the preferable option for the case study structure.

### 3. ACM-Based Retrofit Solution

The retrofit hypothesis was designed by computing the effects of the ACM-induced active confinement on the compression strength and ultimate strain of concrete. Relevant calculations were carried out by referring to the formulas provided by the Instructions for application of the Italian Technical Standards [56], recapitulated below.

#### 3.1. Beams and Columns

In the following, symbol  $\rho_s$  is assumed to denote the transversal reinforcement volume ratio for discontinuous jacketing made of strips, given by  $\rho_s = 2A_s \cdot (b + h) / (b \cdot h \cdot s)$ , with  $A_s$ ,  $s$  = transversal section and spacing of strips,  $b$ ,  $h$  = RC section sides, and  $f_{ywd}$  the design yielding stress of the constituting stainless steel of strips (equal to 560 MPa for the basic ACM application conceived in this study). Based on this notation, the cylindrical compression strength of the confined concrete,  $f_{cc}$ , is obtained from the unconfined strength,  $f_c$ , as follows:

$$f_{cc} = f_c \cdot \left[ 1 + 3.7 \cdot \left( \frac{0.5 \cdot \alpha_n \cdot \alpha_s \cdot \rho_s \cdot f_{ywd}}{f_c} \right)^{0.86} \right] \quad (1)$$

where:

$$\alpha_n = 1 - \frac{(b - 2R)^2 + (h - 2R)^2}{3b \cdot h} \tag{2}$$

$$\alpha_s = \left(1 - \frac{s - h_s}{2b}\right) \cdot \left(1 - \frac{s - h_s}{2h}\right) \tag{3}$$

with  $h_s$  = strip height and  $R$  = manufacturing smoothing radius, which can be put as equal to:

$$R = \min(L_{ang}; 5t_{ang}) \tag{4}$$

where  $L_{ang}$ ,  $t_{ang}$  are the side and thickness of the steel angles. The  $\epsilon_{cc}$  strain at the peak stress and the  $\epsilon_{ccu}$  ultimate strain of confined concrete are derived from the corresponding  $\epsilon_c$  and  $\epsilon_{cu}$  values in original unconfined conditions by means of the following relations:

$$\epsilon_{cc} = \epsilon_c \cdot \left[1 + 5 \left(\frac{f_{cc}}{f_c} - 1\right)\right] \tag{5}$$

$$\epsilon_{ccu} = \epsilon_{cu} + 0.5 \cdot \frac{0.5\alpha_n \cdot \alpha_s \cdot \rho_s \cdot f_{ywd}}{f_{cc}} \tag{6}$$

When the intervention was designed, a decision was made to place the steel strips at the ends of each column in unsafe conditions, with the number of layers ranging from two to four, and constant spacing of 50 mm or 100 mm. For unsafe beams, two strip layers with a spacing of 100 mm were always adopted. The columns and beams subjected to the interventions are identified with different colours in the structural plans drawn in Figures 13–16. Therein, the labels “Full height ACM-strengthened” (in green) and “Web ACM-strengthened” (pink) mean that the lateral side of the strips is either limited to the out-of-depth portion of beams or extended to their whole height.

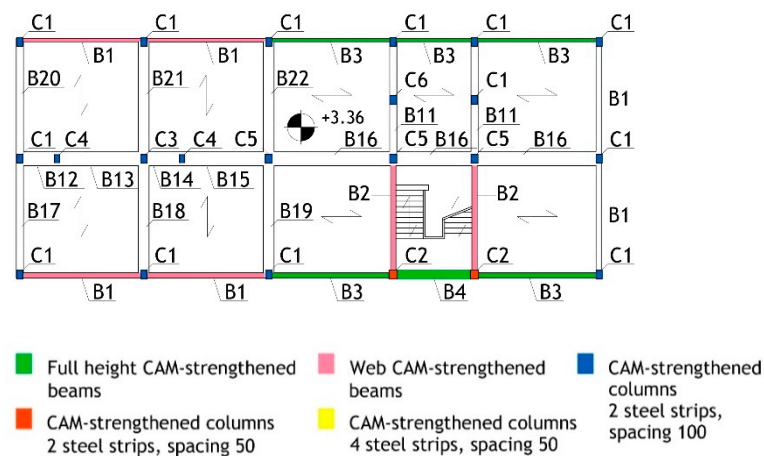


Figure 13. Localization of the interventions—ground storey—and nomenclature for all storeys.

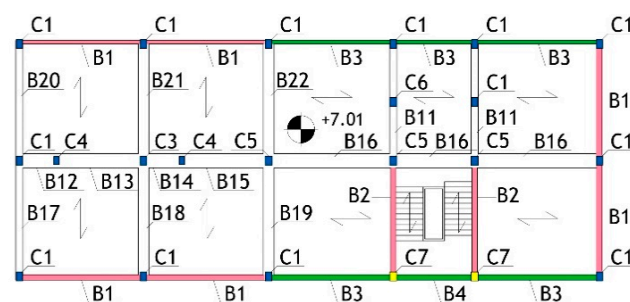


Figure 14. Localization of the interventions—first storey.

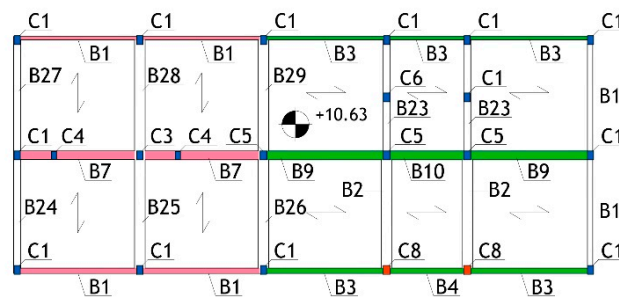


Figure 15. Localization of the interventions—second storey.

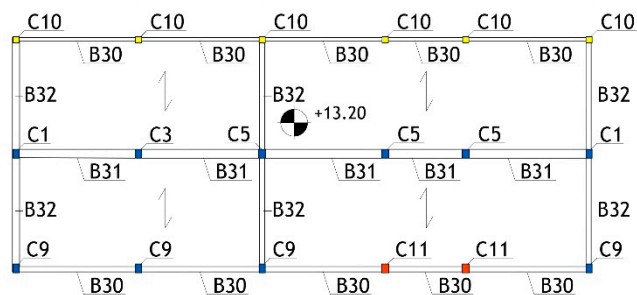


Figure 16. Localization of the interventions—third storey.

The  $f_{cc}$ ,  $\epsilon_{cc}$ , and  $\epsilon_{ccu}$  values computed by means of Formulas (1), (5) and (6), respectively, are recapitulated in Table 1, for the columns subjected to the intervention, and Table 2, for beams. The  $f_{cc}$  values are about 10% to 50% greater than the  $f_c$  value of 20.3 MPa identified in current conditions, as mentioned in Section 2.1; at the same time,  $\epsilon_{cc}$  and  $\epsilon_{ccu}$  are about 180% to 415% greater than the corresponding  $\epsilon_c$  and  $\epsilon_{cu}$  values of 0.00156 and 0.00402, respectively, cited in Section 2.1 as well.

Table 1. Mechanical parameters of confined concrete—columns.

Column Type	Strips (Layers/Spacing)	$f_{cc}$ (MPa)	$\epsilon_{cc}$	$\epsilon_{ccu}$
C1	2/100 mm	22.65	0.00314	0.01136
C2	2/50 mm	24.77	0.00413	0.01859
C3	2/100 mm	22.67	0.00315	0.01141
C4	2/100 mm	22.92	0.00327	0.01231
C5	2/100 mm	22.59	0.00311	0.01113
C6	2/100 mm	22.59	0.00311	0.01113
C7	4/50 mm	28.58	0.00606	0.03072
C8	2/100 mm	24.88	0.00423	0.01914
C9	2/100 mm	23.25	0.00343	0.01348
C10	4/50 mm	31.31	0.00739	0.03813
C11	2/50 mm	25.92	0.00474	0.02257

Table 2. Mechanical parameters of confined concrete—beams.

Beam Type	Strips (Layers/Spacing)	$f_{cc}$ (MPa)	$\epsilon_{cc}$	$\epsilon_{ccu}$
B1	2/100 mm	23.79	0.0037	0.01541
B2	2/100 mm	24.14	0.00385	0.01663
B3/B4	2/100 mm	23.43	0.00352	0.01414
B7	2/100 mm	22.58	0.0031	0.01109
B9/B10	2/100 mm	22.57	0.00302	0.01048

The confinement effects in terms of moment-curvature response are demonstratively visualised in Figure 17 for column C1. Consistently with the results obtained for the compression strength and ultimate strain values, the diagram highlights an increase in peak moment and ultimate curvature equal to about 15% and 160%, respectively. This underlines a considerable improvement of bending moment capacity and a very high growth in ductility reached, thanks to the ACM-induced confinement action.

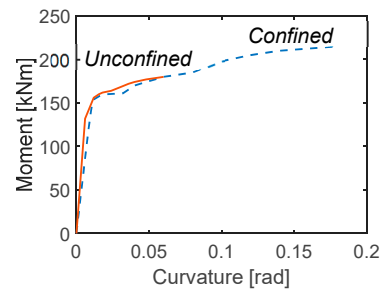


**Figure 17.** Bending moment-curvature diagram for C1 column referred to its strong flexural axis.

The bending moment (beams) and axial force-biaxial bending moment (columns) checks in retrofitted conditions were developed by replacing the original properties of concrete with the corresponding ones of confined concrete, for each strengthened member. The results of these checks, not reported in detail for brevity's sake, show *DCR* values below one, and, thus, safe conditions, for all beams and columns. Furthermore, plastic demand is reduced by up to 20% in the most stressed members, and by 18% in the complete structure, as highlighted by the hysteretic response of C1 ground storey column in Figure 18 and the energy time-histories in Figure 19, which replicate in retrofitted conditions the corresponding graphs plotted in Figures 11 and 12 for the current state. The reduction in the plastic demand is a consequence of the increased elastic response limits of beams and columns produced by the intervention, in addition to the enhancement of their strength capacities.

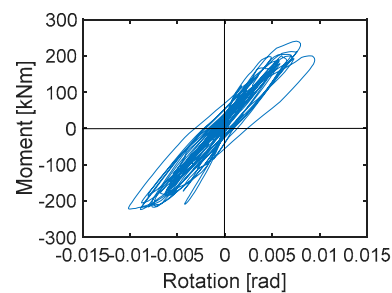


**Figure 18.** Bending moment-rotation response of C1 ground storey column belonging to A5 alignment around its strong flexural axis in retrofitted conditions.

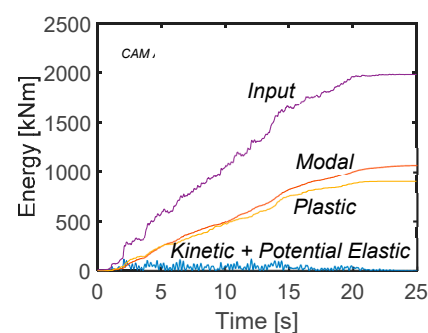


**Figure 19.** Energy time-histories of the structure in retrofitted conditions.

In order to develop shear checks on beams and columns, the contribution of the ACM system strips,  $V_{Rsd,ACM}$ , to the tensile shear strength was evaluated as follows [56]:

$$V_{Rsd,ACM} = 0.9 \cdot d \cdot \frac{2t_s}{s} \cdot b_s \cdot 0.5 f_{ywd} \cdot \cot\theta \quad (7)$$

where  $d$  is the effective depth of the RC section,  $t_s$  and  $b_s$  are the thickness and width of strips, 0.5 is a reduction factor adopted to guarantee an elastic response of strips—and thus their effectiveness in limiting concrete crack width—with considerable margin, and  $\theta$  is the angle of inclination of shear cracks with respect to the horizontal. In retrofitted conditions, the resultant shear strength in tension,  $V_{Rsd,r}$ , is given by the sum of  $V_{Rsd,ACM}$  and the value in current state,  $V_{Rsd,c}$ .  $V_{Rsd,c}$ ,  $V_{Rsd,ACM}$ , and  $V_{Rsd,c}$  are lower than the corresponding values of the shear strength in compression,  $V_{Rcd,ACM}$  and  $V_{Rcd,c}$ , computed by considering, in relevant formulas,  $f_c$  in current state, and  $f_{cc}$  in retrofitted conditions. Therefore, the tensile values  $V_{Rsd,c}$  and  $V_{Rsd,r}$  were assumed in the stress state checks as shear strength measures. Relevant values are recapitulated in Tables 3 and 4 for the most stressed columns and beams, along with the shear demand values derived from the analysis,  $V_{Ed}$ , and the  $DCR$  values in current and retrofitted conditions,  $DCR_c$  and  $DCR_r$ . As highlighted by Tables 3 and 4, all members reach safe post-retrofit shear stress states, with the maximum  $DCR_r/DCR_c$  ratios (which give a direct measure of the maximum performance enhancement obtained thanks to the ACM-based intervention) ranging from about 2.8, for beams, to about 10, for columns.

**Table 3.** Shear demand, capacity values in current and retrofitted conditions, and relevant demand/capacity  $DCR$  ratios—selected columns.

Column	Storey	$V_{Ed}$ (kN)	$V_{Rsd,c}$ (kN)	$V_{Rsd,r}$ (kN)	$DCR_c$	$DCR_r$
C1	Ground	113.4	59.8	275.3	1.90	0.41
C2	Ground	287.2	99.7	530.6	2.88	0.54
C4	Ground	105.2	53.6	247.5	1.96	0.43
C1	1	85.6	59.8	275.3	1.43	0.31
C3	1	110.4	74.7	290.2	1.48	0.38
C4	1	82.6	66.9	260.9	1.23	0.32
C7	1	186.9	78.9	653.7	2.37	0.29
C8	2	117.9	78.9	423.6	1.49	0.28
C10	3	143.7	41.1	435.2	3.49	0.33

**Table 4.** Shear demand, capacity values in current and retrofitted conditions, and relevant demand/capacity  $DCR$  ratios—selected beams.

Beam	Storey	$V_{Ed}$ (kN)	$V_{Rsd,c}$ (kN)	$V_{Rsd,r}$ (kN)	$DCR_c$	$DCR_r$
B1	Ground	137.8	72.3	192.9	1.91	0.71
B2	Ground	125.6	59.8	137.4	2.60	0.91
B1	1	121.5	72.3	192.9	1.68	0.63
B2	1	132.1	59.8	137.4	2.36	0.96
B7	2	84.5	59.8	167.5	1.41	0.51

The design drawings of the interventions on beams, both for the case of “Full height” and “Web” ACM-strengthened ones, and columns are illustrated in Figures 20–22.

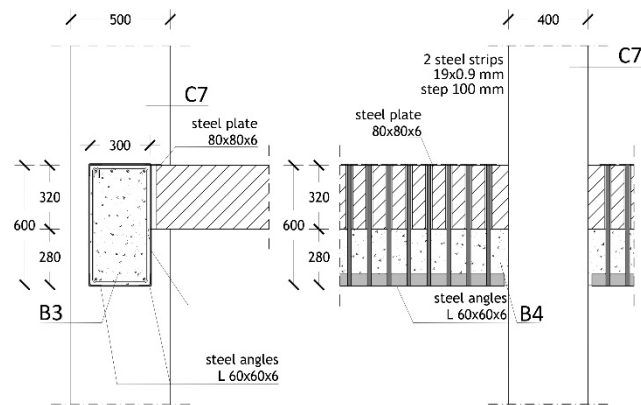


Figure 20. Full height ACM-strengthened beam.

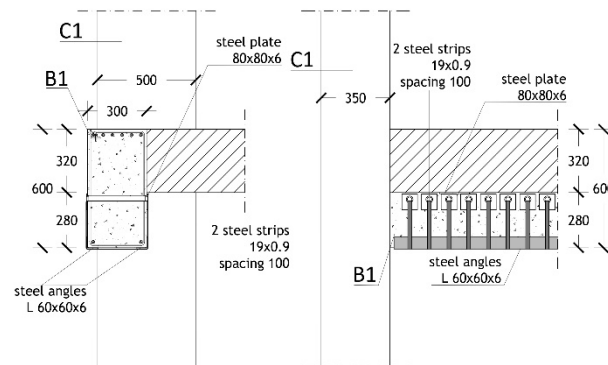


Figure 21. Web ACM-strengthened beam.

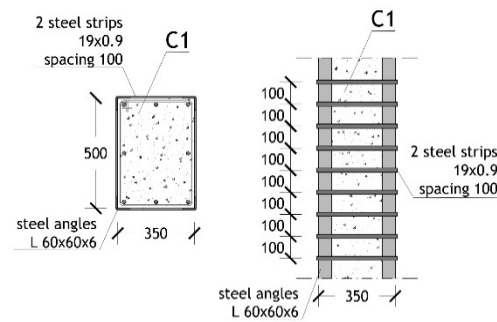


Figure 22. ACM-strengthened column.

### 3.2. Beam-to-Column Joints

Stress checks were carried out on all beam-to-column joints, as none of them meet the condition of a geometrically confined joint. According to [56], the two possible collapse mechanisms were evaluated, i.e., in tension and compression, showing that—as mentioned in Section 2—25 out of 60 joints are in unsafe conditions in the current state, with the maximum demand/capacity ratios of 2.74. Based on these results, the ACM system was applied to the unsafe joints too. The checks were replicated in retrofitted configuration, by means of the following relations:

$$\sigma_{nt} = \left| \frac{N}{2A_j} + \frac{\sigma_h}{2} - \sqrt{\left( \frac{N}{2A_j} + \frac{\sigma_h}{2} \right)^2 + \left( \frac{V_n}{A_j} \right)^2} \right| \leq 0.3\sqrt{f_{cc}} \quad (8)$$

$$\sigma_{nc} = \frac{N}{2A_j} + \frac{\sigma_h}{2} + \sqrt{\left(\frac{N}{2A_j} - \frac{\sigma_h}{2}\right)^2 + \left(\frac{V_n}{A_j}\right)^2} \leq 0.5f_{cc} \quad (9)$$

where  $\sigma_{nt}$  and  $\sigma_{nc}$  are the principal tensile and compressive stresses,  $N$  is the axial force in the column above the joint,  $A_j$  is the area of the joint surface evaluated for the direction along which shear is considered,  $V_n$  is the total shear acting on the joint (given by the sum of the shear transmitted by the column above and the horizontal forces transferred by the upper face of the concurrent beams), and  $\sigma_h$  is the horizontal active confinement pressure exerted by the strips placed on the joint, expressed as follows:

$$\sigma_h = \frac{n_c \cdot n_s \cdot 2 \cdot A_s \cdot f_{ywd}}{b_j \cdot h_{jw}} \quad (10)$$

where  $n_c$  is the number of strip positions in the joint,  $n_s$  is the number of layers per each strip, and  $b_j$  and  $h_{jw}$  are the effective width and height of the joint. The same type of strips as used to strengthen beams and columns was adopted for joints too. The spacing and number of layers per strip were calculated for each unsafe joint in current state by means of expressions (8)–(10). The design drawings of the intervention on the most stressed corner and perimeter joint, both situated in the ground storey and denoted with letters “B” and “N” in Figure 23, are illustrated in Figures 24 and 25. The quantity of strips requested for ground storey joint N (10 strip layers with 50 mm spacing) is the same as for the adjacent joint “O”. All remaining perimeter joints are strengthened with a lower number of strips (from eight to two layers, and with spacing of 50 mm or 100 mm).

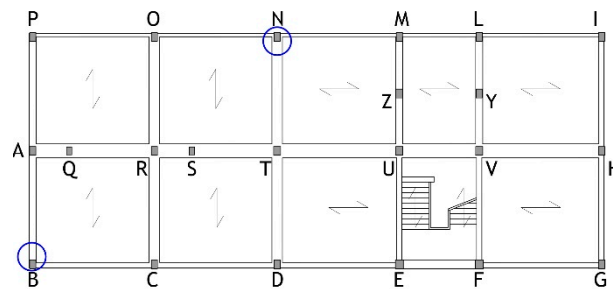


Figure 23. Numbering of beam-to-column joints.

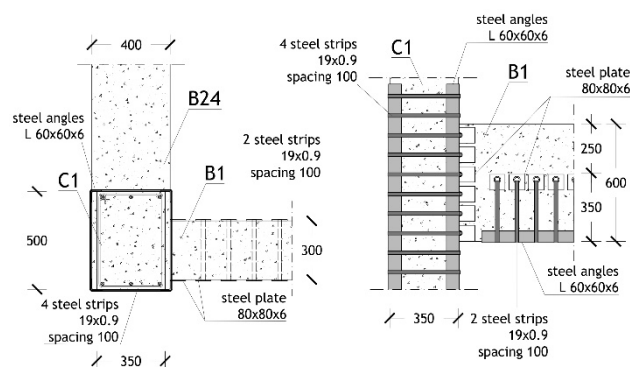


Figure 24. ACM-strengthened ground storey beam-to-column joint B.

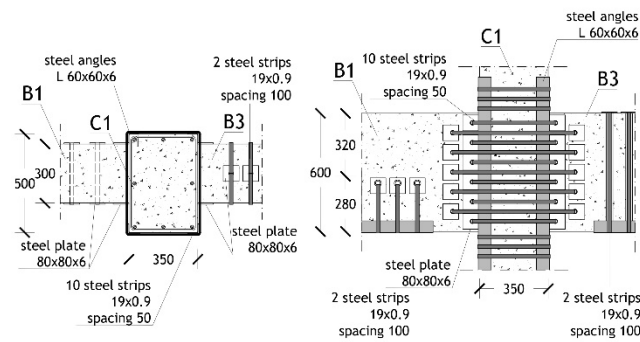


Figure 25. ACM-strengthened ground storey beam-to-column joint N.

The pre- and post-strengthening demand/capacity ratios for a selected set of most stressed joints, listed in Table 5, highlight that safe stress states are reached in retrofitted conditions, like for beams and columns.

Table 5. Demand/capacity DCR ratios—selected beam-to-column joints.

Joint Type	Storey	$DCR_c$	$DCR_r$
C	1	2.25	0.97
H	1	2.00	0.96
N	1	2.23	0.94
O	1	1.95	0.93
P	1	1.47	0.89
B	2	2.74	0.99
E	2	2.25	0.90
F	2	2.14	0.94

The cost of the structural intervention, demolition, and reconstruction of the involved portions of façade infills and partitions included, amount to about 150 Euro/m<sup>2</sup>, i.e., 25–30% lower than the cost estimated for traditional retrofit strategies, like RC-based jacketing of beams, columns and joints, incorporation of additional earthquake-resistant structural members, etc. The latter strategy would also considerably increase the lateral stiffness of the structure, which is not motivated by the displacement performance in current state and, at the same time, could cause an unfavourable growth of storey shears.

Finishes, like plasters, paintings, and floor tiles are not included in cost computation, as they are included in the architectural renovation works planned for the building. At the same time, no interference with the thermal and electrical plants—and thus no additional related cost—is determined by the installation of the ACM system.

#### 4. Conclusions

The study on the application of the ACM system to reinforced concrete structures presented in this article was aimed at evaluating, for a real building, all the aspects involved in the practical design of this retrofit strategy, as well as the actual levels of seismic improvement that it can offer. Indeed, although the use of the ACM was extended to RC structures several years ago, the literature on this technology is essentially limited to technical reports focused on the calculation of the interventions on single members, and relevant installation details.

The case study selected for this research is representative of the wide class of RC buildings designed in the 1960s without anti-seismic provisions, which causes a considerable earthquake-related vulnerability even when they are characterised by geometrical regularity and a simple and clearly conceived structural organization, like the examined school.

The results of the assessment analyses and the development of the ACM-based design hypothesis are summarised in the concluding remarks listed below.

- The response of the structure at the BDE level of seismic action highlights unsafe shear stress states in most beams and columns, with the maximum demand/capacity ratios reaching 2.6 in the former and 3.49 in the latter. Furthermore, about 40% of beams do not meet stress checks in flexure, and more than 50% of columns in normal force/biaxial flexure. About 40% of beam-to-column joints are in unsafe conditions too.
- On the other hand, thanks to the structural regularity of the building and to its low number of storeys, the response in terms of inter-storey drifts is not so poor.
- As a consequence of the combined stress states/drifts assessment, a local strengthening strategy, like the ACM, was evaluated as the preferable retrofit choice for the building.
- Thanks to the active confinement action offered by this technology, the intervention allows reaching a safe response of all members. This is obtained with a relatively small number of strips in all beams (two strip layers with 100 mm spacing) and columns (characterised by the same design output, except for two elements, where four strip layers and a 50 mm spacing are requested).
- A comparable quantity of strips is computed for most beam-to-column joints, except for the perimeter ones, where the number of strip layers exceptionally reaches a maximum of 10 for two of them, situated on the ground storey, and eight or six in four other perimeter joints. This is due to the total absence of stirrups and of any type of transversal reinforcement in the joints, which is typical of the RC structures of the time, causing a remarkably poor response capacity in tension in the most stressed ones.
- In addition to the effects on strength, the confinement action supplied by the ACM produces remarkable benefits in terms of ductility as well, as quantified by an increase in ultimate curvature in columns always greater than 100%, with the peak of 160%.
- The reliable cost analysis of a complete building offered in this study allowed an estimation of the amount of structural works which was 25–30% lower than the cost typically associated to traditional retrofit strategies. This is owed to fewer demolitions, as well as to quicker installation times required by the ACM.
- The localization of the intervention inherent to this retrofit strategy, and the practically null increase in the strengthened RC member sections, helps to avoid any appreciable increase in the lateral stiffness of the structural system, and, thus, any related growth in storey shears.
- The combined seismic performance enhancement/cost evaluation obtained as a final result of the study confirms the opportunity of a wider application of the ACM method to the seismic retrofit of RC frame structures in the next future.

**Author Contributions:** Conceptualization, S.S. and G.T.; methodology, S.S., G.T. and E.F.; software, E.F.; validation, S.S., G.T. and E.F.; formal analysis, G.T. and E.F.; investigation, S.S., G.T. and E.F.; resources, G.T.; data curation, G.T. and E.F.; writing—original draft preparation, S.S. and G.T.; writing—review and editing, S.S. and G.T.; funding acquisition, G.T. All authors have read and agreed to the published version of the manuscript.

**Funding:** Financial support from ReLUIS-DPC Project 2019–2021 (Work Package 15: Normative Contributions for Isolation Project 9—protocol nr. 60–5 February 2019—grant nr. 1100004434, 10.13039/50) is gratefully acknowledged.

**Conflicts of Interest:** The authors declare no conflict of interest.

## Abbreviations

ACM	Active Confinement of Masonry (“CAM” in Italian, registered trademark)
ALC	active lateral confinement
PLC	passive lateral confinement
RC	reinforced concrete
BDE	Basic Design Earthquake
SDE	Serviceability Design Earthquake
DCR	demand/capacity ratio

## References

- Thermou, G.E.; Pantazopoulou, S.J. Assessment indices for the seismic vulnerability of existing R.C. buildings. *Earthq. Eng. Struct. Dyn.* **2011**, *40*, 293–313. [[CrossRef](#)]
- Sorace, S.; Terenzi, G. Structural assessment of a modern heritage building. *Eng. Struct.* **2013**, *49*, 743–755. [[CrossRef](#)]
- Sorace, S.; Terenzi, G. Motion control-based seismic retrofit solutions for a R/C school building designed with earlier Technical Standards. *Bull. Earthq. Eng.* **2014**, *12*, 2723–2744. [[CrossRef](#)]
- Richart, F.A.; Brandtzaeg, A.; Brow, R.L. *A Study of the Failure of Concrete under Combined Compressive Stress*; University of Illinois Engineering Experiment Station Bulletin: Urbana, IL, USA, 1928.
- Kent, D.C.; Park, R. Flexural members with confined concrete. *ASCE J. Struct. Div.* **1971**, *97*, 1969–1990. [[CrossRef](#)]
- Desayi, P.; Iyengar, K.T.S.A.; Reddy, T.S. Equations for stress strain curve of concrete confined in circular steel spiral. *Mater. Struct. Test. Res.* **1978**, *11*, 33945. [[CrossRef](#)]
- Mander, J.B.; Priestley, M.J.N.; Park, R. Theoretical stress strain model for confined concrete. *ASCE J. Struct. Eng.* **1988**, *114*, 1804–1826. [[CrossRef](#)]
- Saatcioglu, M.; Razvi, S.R. Strength and ductility of confined concrete. *ASCE J. Struct. Eng.* **1992**, *118*, 1590–1607. [[CrossRef](#)]
- Uy, B. Strength of reinforced concrete columns bonded with external steel plates. *Mag. Concr. Res.* **2002**, *54*, 61–76. [[CrossRef](#)]
- Li, Y.F.; Chen, S.H.; Chang, K.C.; Liu, K.Y. A constitutive model of concrete confined by steel reinforcements and steel jackets. *Can. J. Civ. Eng.* **2005**, *32*, 279–288. [[CrossRef](#)]
- Gimenez, E.; Adam, J.M.; Ivorra, S.; Calderon, P.A. Influence of strips configuration on the behavior of axially loaded RC columns strengthened by steel angles and strips. *Mater. Des.* **2009**, *30*, 4103–4111. [[CrossRef](#)]
- Montuori, R.; Piluso, V. Reinforced concrete columns strengthened with angles and battens subjected to eccentric load. *Eng. Struct.* **2009**, *31*, 539–550. [[CrossRef](#)]
- Nagaprasad, P.; Sahoo, D.P.; Rai, C.D. Seismic strengthening of RC columns using external steel cage. *Earthq. Eng. Struct. Dyn.* **2009**, *38*, 1563–1586. [[CrossRef](#)]
- Roca, J.G.; Adam, J.M.; Calderon, P.A. Behavior of RC columns strengthened by steel caging under combined bending and axial loads. *Constr. Build. Mater.* **2011**, *25*, 2402–2412. [[CrossRef](#)]
- Wang, L.; Kai-Leung, S.R. Theoretical and experimental study of plate-strengthened concrete columns under eccentric compression loading. *ASCE J. Struct. Eng.* **2013**, *139*, 350–359. [[CrossRef](#)]
- Rodriguez, M.; Park, R. Seismic load tests of reinforced concrete columns strengthened by jacketing. *ACI Struct. J.* **1994**, *91*, 150–159.
- Priestley, N.M.J.; Seible, F.; Xiao, Y.; Verma, R. Steel jacket retrofitting of reinforced concrete bridge columns for enhanced shear strength—Part 2: Test results and comparison with theory. *ACI Struct. J.* **1994**, *91*, 537–548.
- Aboutaha, R.S.; Engelhardt, M.D.; Jirsa, J.O.; Kreger, M.E. Retrofit of concrete columns with inadequate lap splices by the use of rectangular steel jackets. *Earthq. Spectra* **1996**, *12*, 693–714. [[CrossRef](#)]
- Xiao, Y.; Wu, H. Retrofit of reinforced concrete columns using partially stiffened steel jackets. *ASCE J. Struct. Eng.* **2003**, *129*, 725–732. [[CrossRef](#)]
- Kaliyaperumal, G.; Sengupta, A.K. Seismic retrofit of columns in buildings for flexure using concrete jacket. *ISSET Earthq. Techn. J.* **2009**, *46*, 77–107.
- Lin, M.N.; Chen, P.C.; Tsai, K.C.; Yu, Y.J.; Liu, J.G. Seismic steel jacketing of rectangular RC bridge columns for the mitigation of lap splice failures. *Earthq. Eng. Struct. Dyn.* **2010**, *39*, 1687–1710. [[CrossRef](#)]
- Belal, M.F.; Mohamed, H.M.; Morad, S.A. Behavior of reinforced concrete columns strengthened by steel jacket. *HBRC J.* **2015**, *11*, 201–212. [[CrossRef](#)]
- Júlio, E.S.; Branco, F.; Silva, V.D. Structural rehabilitation of columns with reinforced concrete jacketing. *Prog. Struct. Eng. Mater.* **2003**, *5*, 29–37. [[CrossRef](#)]
- Bousias, S.N.; Biskinis, D.E.; Fardis, M.N. Strength, stiffness and cyclic deformation capacity of concrete jacketed members. *ACI Struct. J.* **2007**, *104*, 521–531.
- Vandoros, K.G.; Dritsos, S.E. Concrete jacket construction detail effectiveness when strengthening RC columns. *Constr. Build. Mater.* **2008**, *22*, 264–276. [[CrossRef](#)]
- Sezen, H.; Miller, E.A. Experimental evaluation of axial behavior of strengthened circular reinforced-concrete columns. *J. Bridge Eng.* **2011**, *16*, 238–247. [[CrossRef](#)]

27. Foti, D.; Vacca, S. Mechanical behavior of concrete columns reinforced with rheoplastic mortar. *Mater. Constr./Build. Mater.* **2013**, *63*, 267–282. [[CrossRef](#)]
28. Lorenzis, L.D.; Teffers, R. Comparative study of models on confinement of concrete cylinders with fiber-reinforced polymer composites. *ASCE J. Compos. Constr.* **2003**, *7*, 21937. [[CrossRef](#)]
29. Xiao, Y.; Wu, H. Compressive behavior of concrete confined by carbon fiber composite jackets. *J. Mater. Civ. Eng.* **2000**, *12*, 13946. [[CrossRef](#)]
30. Ilki, A.; Peker, O.; Karamuk, E.; Demir, C.; Kumbasar, N. FRP retrofit of low and medium strength circular and rectangular reinforced concrete columns. *J. Mater. Civ. Eng.* **2008**, *20*, 169–188. [[CrossRef](#)]
31. Rousakis, T.C.; Karabinis, A.I. Adequately FRP confined reinforced concrete columns under axial compressive monotonic or cyclic loading. *RILEM Mater. Struct.* **2012**, *45*, 957–975. [[CrossRef](#)]
32. Mazza, F.; Mazza, M. Seismic retrofitting of gravity-loads designed r.c. framed buildings combining CFRP and hysteretic damped braces. *Bull. Earthq. Eng.* **2019**, *17*, 3423–3445. [[CrossRef](#)]
33. Madotto, R.; Van Engelen, N.C.; Das, S.; Russo, G.; Pauletta, M. Shear and flexural strengthening of RC beams using BFRP fabrics. *Eng. Struct.* **2021**, *229*, 111606. [[CrossRef](#)]
34. Rossi, E.; Randl, N.; Mészöly, T.; Harsányi, P. Flexural strengthening with fiber-/textile-reinforced concrete. *ACI Struct. J.* **2021**, *118*, 97–107.
35. Krstulovic-Opara, N.; Thiedeman, P.D. Active confinement of concrete members with self-stressing composites. *ACI Struct. J.* **2000**, *97*, 297–308.
36. Triantafyllou, T.C. Seismic retrofitting of structures with fibre-reinforced polymers. *Prog. Struct. Eng. Mater.* **2001**, *3*, 57–65. [[CrossRef](#)]
37. Mortazavi, A.; Pilakoutas, K.; Son, K.S. RC column strengthening by lateral pre-tensioning of FRP. *Constr. Build. Mater.* **2003**, *17*, 491–497. [[CrossRef](#)]
38. Saatcioglu, M.; Yalcin, C. External prestressing of concrete columns for improved seismic shear resistance. *ASCE J. Struct. Eng.* **2003**, *129*, 105770. [[CrossRef](#)]
39. Tamuzs, V.; Teffers, R.; Chi-Sang, Y.; Rousakis, T.; Repelis, I.; Skruls, V.; Vilks, U. Behaviour of concrete cylinders confined by carbon-composite tapes and prestressed yarns. 1—Experimental data. *Mech. Compos. Mater.* **2006**, *42*, 13–32. [[CrossRef](#)]
40. Janke, L.; Czaderski, C.; Ruth, J.; Motavalli, M. Experiments on the residual load-bearing capacity of prestressed confined concrete columns. *Eng. Struct.* **2009**, *31*, 2247–2256. [[CrossRef](#)]
41. Andrawes, B.; Shin, M.; Wierschem, N. Active confinement of reinforced concrete bridge columns using shape memory alloys. *ASCE J. Bridge Eng.* **2010**, *15*, 81–89. [[CrossRef](#)]
42. Choi, E.; Nam, T.-H.; Yoon, S.J.; Cho, S.K.; Park, J. Confining jackets for concrete cylinder using NiTiNb and NiTi shape memory alloys wires. *Phys. Scr.* **2010**, *T139*, 014058. [[CrossRef](#)]
43. Shin, M.; Andrawes, B. Experimental investigation of actively confined concrete using shape memory alloys. *Eng. Struct.* **2010**, *32*, 656–664. [[CrossRef](#)]
44. Zuboski, G.R. Stress-Strain Behaviour for Actively Confined Concrete Using Shape Memory Alloys. Master’s Thesis, Department of Civil Engineering, The Ohio State University, Columbus, OH, USA, 2013.
45. Holmes, N.; Niall, D.; O’Shea, C. Active confinement of weakened concrete columns. *Mater. Struct.* **2015**, *48*, 2759–2777. [[CrossRef](#)]
46. Tran, H.; Balandraud, X.; Destrebecq, J.F. Improvement of the mechanical performances of concrete cylinders confined actively or passively by means of SMA wires. *Arch. Civ. Mech. Eng.* **2015**, *15*, 292–299. [[CrossRef](#)]
47. Fakharifar, M.; Chen, G.; Wu, C.; Shamsabadi, A.; ElGawady, M.A.; Dalvand, A. Rapid repair of earthquake-damaged RC columns with prestressed steel jackets. *J. Bridge Eng.* **2016**, *21*, 4015075. [[CrossRef](#)]
48. Abdelrahman, K.; El-Hacha, R. Experimental investigation of RC columns confined with Ni–Ti shape memory alloy wires versus CFRP sheets. *Can. J. Civ. Eng.* **2021**, *48*, 925–940. [[CrossRef](#)]
49. Dolce, M.; Nigro, D.; Ponzo, F.C.; Marnetto, R. The CAM system for the retrofit of masonry structures. In Proceedings of the 7th International Seminar on Seismic Isolation, Passive Energy Dissipation and Active Control of Vibrations of Structures, Assisi, Italy, 2–5 October 2001; p. 9.
50. Marnetto, R.; Vari, A.; Leonori, M. *Il Sistema CAM—Consolidamento Strutturale Con Cuciture Inox*; 21mo Secolo: Milan, Italy, 2017. (In Italian)
51. Dolce, M.; Nicoletti, M.; De Sortis, A.; Marchesini, S.; Spina, D.; Talanas, F. Osservatorio Sismico delle Strutture: The Italian structural seismic monitoring network. *Bull. Earthq. Eng.* **2017**, *15*, 621–641. [[CrossRef](#)]
52. Dipartimento della Protezione Civile. Available online: <https://www.protezionecivile.gov.it> (accessed on 22 September 2021).
53. SAP2000NL. *Theoretical and Users’ Manual*; Computers & Structures Inc.: Berkeley, CA, USA, 2021.
54. Takeda, T.; Sozen, M.A.; Nielsen, N.N. Reinforced concrete response to simulated earthquakes. *ASCE J. Struct. Div.* **1970**, *96*, 2557–2573. [[CrossRef](#)]
55. Ministry of Infrastructure and Transport. *Update of Technical Standards for Constructions*; Ministerial Decree, 17 January 2018, Ordinary supplement to G.U. no. 42, 20 February 2018; Ministry of Infrastructure and Transport: Rome, Italy, 2018. (In Italian)
56. Ministry of Infrastructure and Transport. *Instructions for the application of the Update of Technical Standards for Constructions*; Circular no. 7, 21 January 2019, Ordinary supplement to G.U. no. 35; Ministry of Infrastructure and Transport: Rome, Italy, 2019. (In Italian)